UK Atomic Energy Authority

UKAEA-STEP-PR(24)17

A. J. Leide, W. Zhong, I. Fernandez-Victorio, D. Nguyen-Manh, T. Koyanagi, A. Gandy

Effect of microstructure and neutron irradiation defects on deuterium retention in SiC

Effect of microstructure and neutron irradiation defects on deuterium retention in SiC

A. J. Leide, W. Zhong, I. Fernandez-Victorio, D. Nguyen-Manh, T. Koyanagi, A. Gandy

This is a preprint of a paper submitted for publication in Frontiers in Nuclear Engineering

Effect of microstructure and neutron irradiation defects on deuterium retention in SiC[1*]

Alex Leide[1*], Weicheng Zhong[2], Isabel Fernandez-Victorio[1,3], Duc Nguyen-Manh[1,3], Takaaki Koyanagi[2], Amy Gandy[1]

[1] *United Kingdom Atomic Energy Authority, Culham Campus, Abingdon, UK*

[2] *Materials Science and Technology Division, Oak Ridge National Laboratory, USA*

[3]*Department of Materials, University of Oxford, Oxford, UK*

Abstract

Retention of hydrogen isotopes is a critical concern for operating fusion reactors as retained tritium both activates components and removes scarce fuel from the fuel cycle. Radiation-induced displacement damage in SiC may influence the retention of hydrogen isotopes compared to pristine SiC. Deuterium retention in neutron irradiated high purity SiC has been compared to different microstructures of non-irradiated high purity SiC using thermal desorption spectroscopy after gas charging or low energy ion implantation. First principles calculations have been conducted to help interpret results and derive effective diffusivity of hydrogen isotopes in SiC in the presence of vacancies. Deuterium is released at lower temperatures in neutron irradiated SiC compared to pristine SiC, suggesting weaker trapping by radiation-induced carbon vacancies compared to at grain boundaries in the pristine samples.

Low energy ion implanted samples had a high deuterium release temperature suggesting C-H bonding associated with ion irradiation induced displacement damage.

1. Introduction

Commercial fusion reactors are reliant on a hydrogen fuel cycle, along with the issues this poses around containing and transporting hydrogen including the radioactive tritium isotope and deuterium [1]. Minimising tritium trapped in the reactor components is vital to ensure sufficient tritium is available in the fuel cycle, and to minimise the radioactivity of components caused by retained tritium [2]. Therefore, an understanding of the retention behaviour of hydrogen isotopes is important for successful reactor operations.

Silicon carbide and its fibre reinforced composites can operate in radiation environments even at ~1000 °C, enabling the breeder blanket of a fusion reactor to generate useful process heat and utilise efficient thermodynamic electricity generating cycles [3–5]. As well as extracting energy, a fusion reactor breeder blanket must create tritium from the interaction of fusion neutrons with lithium, which can be contained in the breeder blanket in a variety of forms including molten lithium, lead-lithium alloy, a molten salt such as FLiBe, or as a solid ceramic breeder [6–8]. The breeder material is one source of tritium generation within a blanket component from which it may enter a silicon carbide structural component via adsorption and diffusion.

A second source of hydrogen in SiC is by transmutation of silicon and carbon atoms. In particular, via the (n,p) reactions which have an energy threshold of 4 MeV for silicon and 13.6 MeV for carbon [9]. Although helium dominates the gaseous transmutation production via the (n,n'3α) reactions with carbon atoms, several thousand parts per million of hydrogen atoms will be generated internally from silicon [10]. The synergistic effects of transmutation defects

with displacement damage and hydrogen isotopes is an ongoing area of research in fusion materials.

Although monolithic SiC is not commonly considered as a plasma facing component due to poor thermal shock resistance, it does have certain benefits for plasma-material interactions as low atomic mass elements radiate less heat when they contaminate the plasma, and sputtering yield is lower than graphite components [11,12]. With further maturity of SiC fiber-reinforced SiC matrix (SiC_f/SiC) composites as a way to mitigate thermal shock behaviour, SiC plasma facing components are gaining renewed interest. Hydrogen isotopes can be introduced to plasma facing components by direct ion implantation from the plasma, or by co-deposition of sputtered material which is transported around the tokamak's magnetic field. Thermodynamics and trapping mechanisms for tritium in plasma facing materials are vital to understand for the purposes of tritium accountancy and detritiation methods for handling and disposal [13].

Previous studies investigated deuterium retention in a range of SiC materials by low energy implantation with deuterium ions followed by thermal desorption spectroscopy (TDS) to measure the deuterium release rate as a function of temperature. Oya identified four peaks in the thermal desorption spectrum of deuterium implanted SiC, claiming the peak at 450 K corresponds to deuterium adsorbed on the surface, 650 K to interstitial deuterium, 800 K for Si-D trapped deuterium, and 1000 K for C-D trapped deuterium [14]. Sugiyama identified 3 different peaks in their deuterium desorption experiments and related these to deuterium trap energies by repeating TDS experiments at different heating rates [15]. These were at higher temperatures than found by Oya; attributing the 800 K peak to Si-D bond, and the 1200 K peak to C-D bond with the 1080 K peak related to C-D trapping in helium pre-implanted carbon-rich regions, i.e. a region with displacement defects.

TDS results also appear to be a function of the implantation temperature, energy, and fluence, with different researchers identifying different numbers of peaks, or desorption rate peaks at different temperatures, making interpretation and comparison very difficult [15–18]. The deuterium ion fluences typically used for experiments in the literature are vast; between 10^{21} and 10^{24} D/m^2 with energy between 0.5 and 50 keV [14,16–20]. Such high fluences are used as most deuterium is spontaneously desorbed rather than being trapped, and these experiments are intended to saturate trapping sites ahead of the TDS measurements. However, ion implantation also causes atomic displacements which will alter the microstructure of the target material. The threshold displacement energy for carbon and silicon atoms is 21 eV and 35 eV respectively, far lower than the threshold displacement energy for tungsten (90 eV) which is what most experimental parameters are based on [21,22]. Koller *et al.* identified a fluence of ~5×10^{21} D/m^2 to achieve saturation of deuterium in SiC for their experiments, and used a fluence of 1×10^{24} D/m^2 for most of their experiments [17]. SRIM estimates of the displacements per atom (dpa) for SiC predict >10 dpa to achieve the "saturation" fluence and that the majority of their experiments imparted 1500 peak dpa to the specimens during ion implantation[17,23]. Most deuterium implantations are conducted at room temperature where SiC is easily amorphized, with a critical temperature threshold between 300 K and 500 K depending on radiation type [24–26]. Above the critical amorphisation temperature, neutron irradiation defects in SiC are strongly temperature dependent, with a decreasing defect density (related to swelling) with increasing irradiation temperature, saturating at less than ~2 dpa [27]. Considering the high implantation doses used in the literature and the displacement damage this creates, the measured deuterium trapping properties will be from a damaged microstructure rather than a pristine microstructure. The effect of helium pre-implantation was investigated by Sugiyama *et al.*, finding higher trapping energies for C-D bonds and a fluence-dependent trapping energy for Si-D trap sites compared to deuterium implantation alone; however, having

found that helium irradiation changes desorption behaviour, the effect of displacement defects was not evaluated [15].

A significant knowledge gap is the interaction of hydrogen isotopes with carbon atoms in SiC through forming covalent hydrocarbon bonds. Under irradiation at elevated temperatures, displacement events form a wide range of crystallographic defects including vacancies and interstitials, plus anti-site defects [28]. In terms of interatomic bonds, these crystallographic defects correspond to the accumulation of chemical disorder by breaking heteronuclear Si-C bonds and forming homonuclear Si-Si and C-C bonds. These bonds are regularly observed in Raman spectroscopy measurements of irradiated SiC, and in first principles calculations of defects which identify carbon bonding signals as coming from carbon clusters or chains with both sp^2 and sp^3 bonding [29–31]. This creates a complex variety of atomic environments and interatomic bonding states to which hydrogen isotopes can bond.

This study investigates the effect of microstructure on the retention of deuterium in high purity polycrystalline cubic SiC, and for the first time the impact of neutron irradiation-induced defects on deuterium retention. Comparative studies are made between deuterium gas charging, and low energy ion implantation. These experimental results are discussed and interpreted in relation with the binding energies of hydrogen in vacancies obtained from first principles calculations. This is a step towards understanding the transport of hydrogen isotopes in SiC components of a fusion power station.

2. Experimental

Materials

Different grades of SiC were studied to investigate the effects of as-fabricated microstructure on deuterium retention. A high-resistivity grade 4H single crystal SiC was obtained from MSE supplies LCC. The nominal impurities included 15 appm Al, 13 appm Fe,

28 appm Zn, and 15 appm K. The primary surface was parallel to the (0001) plane. Two types of polycrystalline chemical vapor deposited (CVD) 3C-SiC material were also tested; high-resistivity grade from Coorstek (CT) contained a high density of stacking faults and a mean grain size of 8 μm, and a specimen of from Rohm and Haas (RH) with a lower density of stacking faults and a 12 μm average grain size. Both samples have a range of grain sizes: RH appears to have a larger "coarse" grain size, and smaller "fine" grain size than CT. EBSD images of the CVD materials are shown in Figure 1 to demonstrate the differences in microstructure, along with a TEM image showing the high stacking fault density in CT. Both materials had nominal metallic purity above 99.9995% based on the vendor's material data sheet. Non-metallic impurities of N and O were determined by secondary ion mass spectrometry at Eurofins EAG Materials Science, LLC: 5 appm N and 2 appm O for single crystal 4H-SiC, 0.1 appm N and 4 appm O for RH SiC, and 0.1 appm N and 10 appm O for CT SiC. The as-fabricated material microstructures have been investigated in the previous study [32].

A nuclear grade of SiC/SiC composite consisting of Hi-Nicalon Type-S (HNS) fibres, a PyC fibre interphase coating, and a chemical vapour infiltrated (CVI) SiC matrix was studied. The material was fabricated at Rolls-Royce High Temperature Composites Inc. (lot number: 13C-529). The fiber architecture was 2D satin-weave, 0°/90° stacking. The thickness of PyC interphase was around 100 nm. The fiber volume fraction and porosity were ~37% and ~13%, respectively. The representative surface microstructure is presented in Figure 1 (d).

A neutron irradiated specimen of Rohm and Haas (RH) CVD SiC of identical grade to the unirradiated material described above was used to investigate the effects of radiation defects on deuterium retention. This specimen was irradiated in the High Flux Isotope Reactor at ORNL to a nominal fluence of 2.24×10^{25} n/m^2 (E>0.1 MeV) ~2.24 displacements per atom. Post-irradiation dilatometry measurement of passive SiC thermometry [33] indicated an

irradiation temperature of ~950 °C. Although the dilatometry method is not practically applied to very high irradiation temperature (>~1000 °C), this study detected subtle recovery of length during annealing (e.g., indication of irradiation temperature). This specimen was chosen as the irradiation temperature is well above the deuterium charging temperature so will minimise defect annealing during gas charging and TDS experiments.

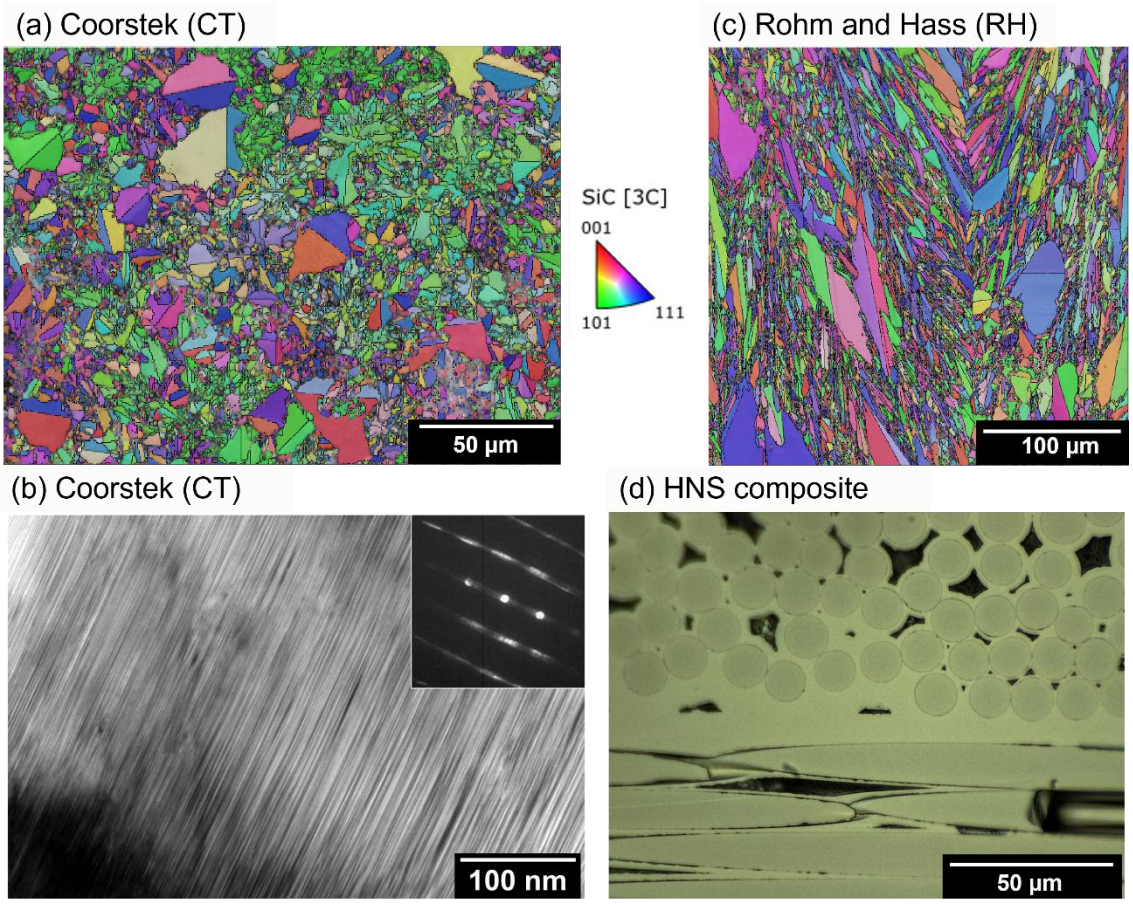

Figure 1: Microstructures of specimens studied in this work. (a) and (c) EBSD orientation maps of CT and RH CVD SiC samples. (b) TEM image of CT showing high stacking fault density. (d) representative optical micrograph of HNS SiC_f/SiC composite.

Deuterium charging, low energy ion implantation, and thermal desorption spectroscopy

Deuterium was introduced to the specimens in two different ways: low energy ion implantation and gas charging by diffusion. Prior to introducing deuterium, all specimens were thermally annealed in vacuum at 900 °C with a 10 °C/minute ramp rate and 1 hour dwell time

to remove any trapped gaseous species. This is below the irradiation temperature therefore microstructural evolution would not be expected to occur in the irradiated specimen.

One ion implantation experiment was conducted on RH SiC to compare the effects of ion implantation and gas charging on microstructure. Implantation was at room temperature, with 10 kV accelerating potential on a D_2^+ charged molecule corresponding to 5 keV/D. The fluence of ions was 5.46×10^{16} D/cm^2. SRIM profiles for atomic concentration and displacements per atom are shown in Figure 2 with an implantation range of ~100 nm, 9.6 at% peak concentration, and 0.61 peak dpa [23]. Threshold displacement energies were 21 eV for carbon atoms and 35 eV for silicon atoms in 3C-SiC, density was 3.21 g/cm^3, and the quick Kinchin-Pease method was used [21,34]. The beam is focussed into a ~1.5 mm diameter area on the specimen.

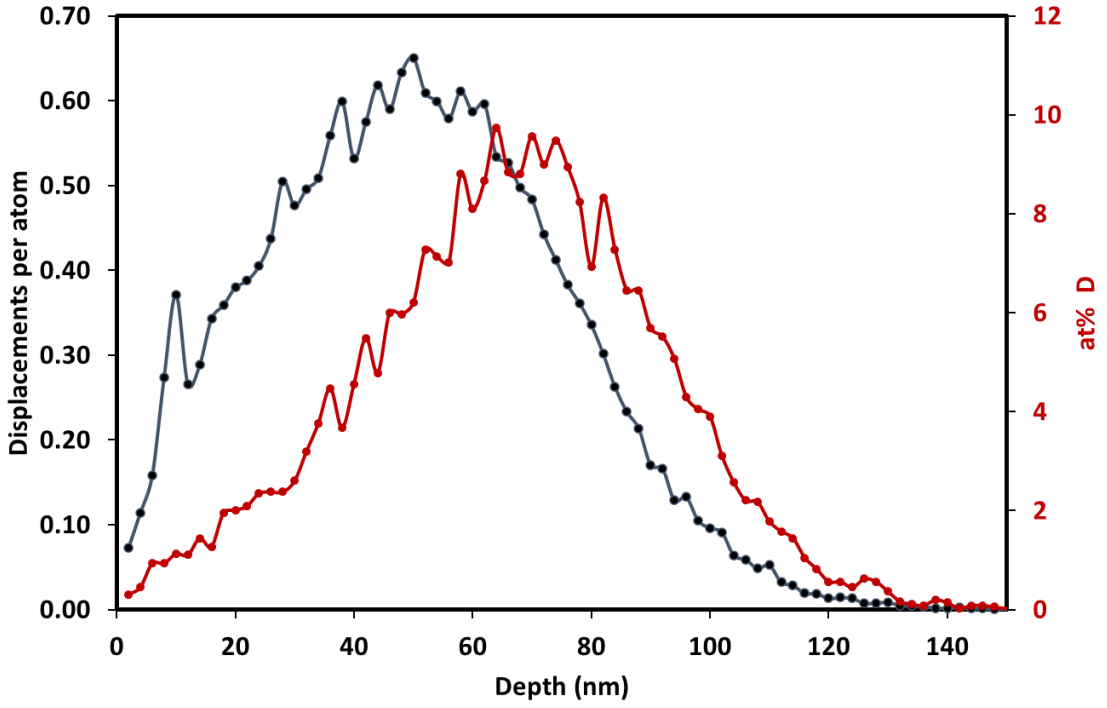

Figure 2: SRIM profiles for 5.46×10^{16} ions/cm^2 5 keV D^+ ion implantation into 3C-SiC.

Gas charging to diffuse deuterium into specimens was carried out in a single-ended quartz tube within an alumina tube furnace. This quartz tube is solely used for deuterium charging experiments to avoid cross contamination. The tube was evacuated and purged with deuterium gas twice before the experiment began. The sample was heated in one atmosphere

of deuterium at 450 °C and held for one hour before cooling. This is below the neutron irradiation temperature therefore microstructural evolution would not be expected to occur. Based on Fick's laws for diffusion from a constant pressure source, and diffusion coefficients calculated by Causey and Wampler for tritium in CVD SiC, a deuterated depth of ~20 nm is predicted, plotted in Figure 3 [35]. These diffusion coefficients and activation energies refer to "vapour deposited SiC", similar to used in this work, are commonly referred to in the literature, however the experimental temperature is higher to enable measurable diffusion depths and rates, which may cause different diffusion mechanisms, therefore this diffusion depth should be considered as an estimate only. This depth is a roughly equivalent range to a 500 eV ion implantation, however does not induce displacement damage to SiC. The atomic concentration of deuterium is lower than achieved by high fluence ion implantation.

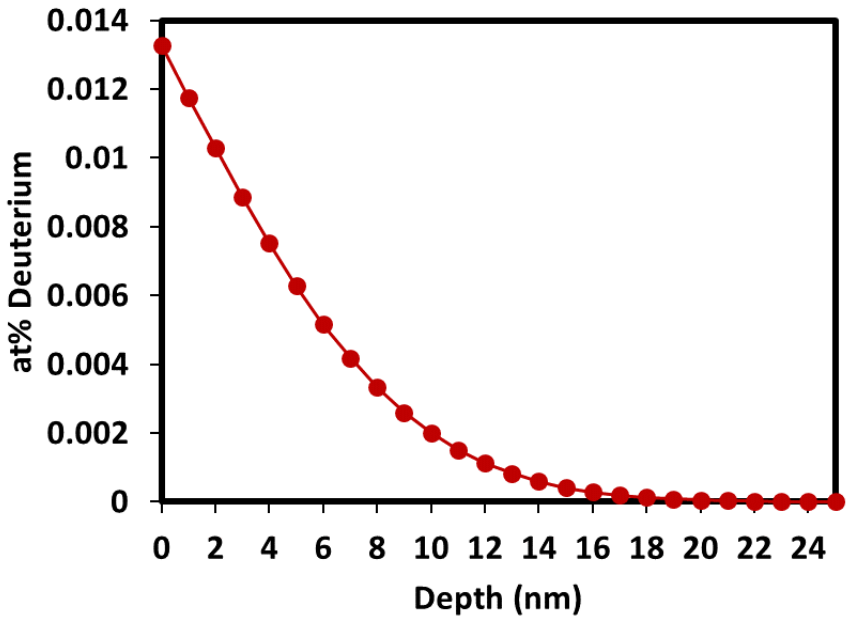

Figure 3: Predicted profile of deuterium diffused into SiC

Thermal desorption spectroscopy (TDS) was carried out in the same tube furnace as used for gas charging experiments, but using a separate quartz tube. The single-ended quartz tube containing the sample was connected to a mass spectrometer and evacuated, followed by heating at 10 °C/min to 900 °C while measuring the outgassing species. TDS experiments were

conducted within one hour of the gas charging experiment. Desorption rates were normalised to the surface area of the specimens measured by digital calliper, and the mass spectrometer was calibrated using standard gas leaks. Contributions to deuterium desorption rate is only reported for mass 4 corresponding to D_2 molecules as this ensures only the intentionally introduced deuterium release is measured and is not influenced by hydrogen background in the experiment. The composite specimen contains open porosity as seen in Figure 1 (d) and therefore a higher surface area than measured by the sample dimensions. For TDS of the ion implantation experiment, the release rate is normalised to the area of the ion implantation.

Raman spectroscopy

Raman spectroscopy was carried out on the deuterium ion implanted RH CVD SiC after thermal desorption spectroscopy. Raman mapping was conducted using a Renishaw inVia confocal Raman microscope with a 532 nm wavelength laser focussed through a 100× objective operated at 30 mW source laser power with a 0.01 s integration time. Spectra were acquired over a 500×500 μm area with 2 μm step size covering a portion of the ion implanted and unimplanted region.

Ab-initio calculations of hydrogen binding and migration energies

Interactions of hydrogen with vacancy defects in silicon carbide were investigated using Density Function Theory (DFT) calculations implemented with Vienna Ab-initio Simulation Package (VASP) [36–38] . The generalized gradient approximation (GGA-PBE) was used for exchange and correlation functional [39] and the acceleration of DFT optimized calculations was achieved by using Projector Augmented Wave (PAW) pseudo-potentials [40]. The Gamma sampling of k points in the Brillouin zone, with k-mesh spacing of 0.2 $Å^{-1}$, was used to calculate the total energies. The plane-wave cut-off energy value of 750 eV has been employed after carefully checking total energy calculations for both primitive cubic and supercell calculations with the convergency of 10^{-5} eV and the force components were relaxed to 10^{-3}

eV/Å. Calculations were performed using the Marconi and Leonardo HPC machines hosted by CINECA, Italy. Formation energies and binding energies were calculated for several situations of hydrogen in defects and interstitial sites, and multiple hydrogen atoms were introduced sequentially to investigate multi-atom trapping. Hydrogen was used for these simulations rather than deuterium. Nudged elastic band calculations were performed to investigate migration barriers along different pathways for interstitial hydrogen in SiC.

Defect formation energy is defined as the energy of the defective system minus the energy of the perfect system minus the sum of the ground state energy of the species added or removed:

$$E_f = E_{total,\ defected} - E_{total,\ perfect} - \sum_i n_i \mu_i \quad (1)$$

where n_i is the number of atoms of species i added (n>0) or removed (n<0) and μ_i is the elemental ground state energy per atom.

Enthalpy of solution for interstitial hydrogen atoms is the total energy of the system including interstitial hydrogen minus the total energy of the perfect crystal cell without hydrogen, minus half the energy of an isolated H_2 molecule:

$$E_s = E_{tot,H} - E_{tot,\ perf} - \frac{1}{2} E_{H_2} \quad (2)$$

Binding energy of a defect cluster $A^n B^m$ which is made up up n defects of type A and m defects of type B is given by:

$$E_b = E_{tot,A^n B^m,} - nE_{tot,A} - mE_{tot,B} + (n + m - 1)E_{tot,perfect} \quad (3)$$

Where a negative value corresponds to attraction between defects. When extra defects are added to a pre-existing defect cluster, the sequential binding energy is used to calculate the binding energy of the extra defect, for example the sequential binding energy of adding a H atom (A) into the defect complex with a vacancy (B) interacting with nH can be written in the formula:

$$E_{b,seq} = E_{tot,H^{n+1}V,} - E_{tot,H} - E_{tot,H^nV} + E_{tot,perfect} \quad (4)$$

3. Results

Thermal desorption spectroscopy results for different grades of SiC which have been gas charged in identical conditions are shown in Figure 4. The HNS-CVI composite has a far higher release rate than the other specimens due to its higher specific surface area, and has been scaled to one tenth of its release rate in the plot. This specimen has a single broad asymmetric desorption peak with a maximum desorption rate at 590 °C. 4H-SiC single crystal has the lowest desorption rate of all the specimens with no distinct peaks, but a broad increase in release rate above 450 °C. Both the RH and CT polycrystalline 3C-SiC specimens have broad peaks with high release rates between 550 °C and ~850 °C. The RH specimen has ~40% higher D_2 release rate than the CT specimen across the temperature range of the D_2 release peak. The shapes of the peaks are also different: CT release rate increases until a maximum at 700 °C before decreasing while the RH release rate is approximately constant between 600 °C and 700 °C before declining. The RH specimen neutron irradiated at 950 °C to 2.24 dpa behaves significantly differently to the pristine RH specimen, showing only a single, sharp desorption rate peak at 550 °C before returning to a low D_2 release rate for the remaining temperature range.

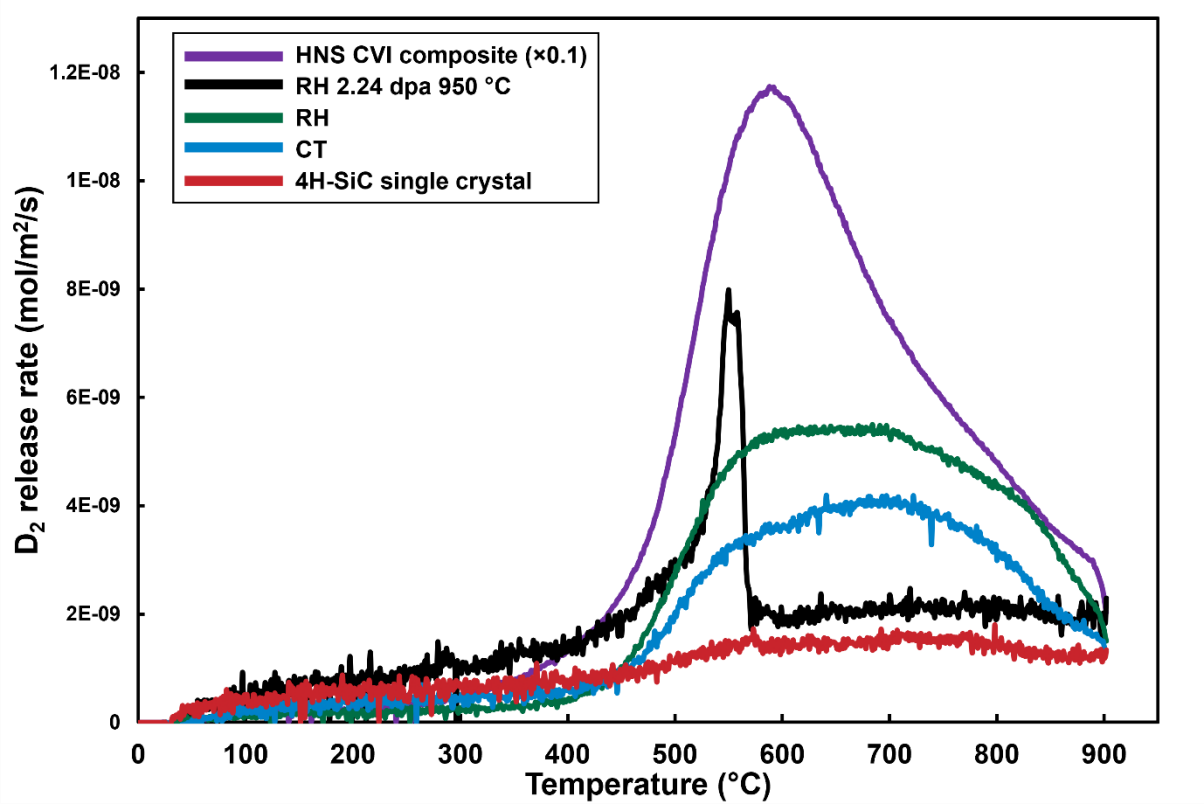

Figure 4: Results for TDS experiments of various microstructures of deuterium gas charging experiments.

Figure 5 shows the TDS results of D_2 release rate from the D_2^+ ion implanted RH specimen. This shows a steadily increasing release rate before a maximum release rate at 850 °C. This desorption rate peak is close to the maximum temperature of these TDS experiments but appears to be falling at the time the experiment ended. The microstructure of this specimen is identical to the RH specimen used for the gas charging experiment, but shows a significantly different desorption profile.

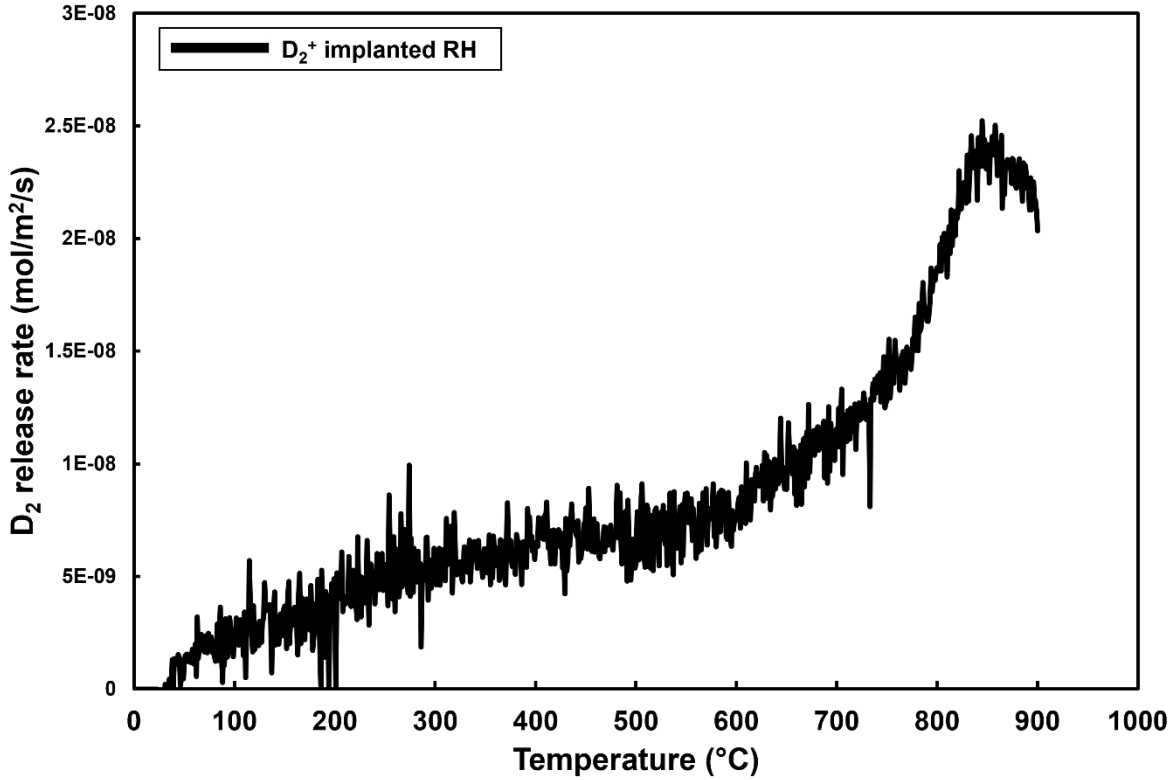

Figure 5: TDS result from D_2^+ ion implanted RH SiC.

Raman spectra comparing pristine non-implanted regions of the RH 3C-SiC specimen and the deuterium implanted region following TDS are shown in Figure 6. As the implantation is very shallow, the majority of the signal arises from underlying unirradiated material explaining the dominance of the TO and LO peaks of 3C-SiC in both spectra. However, following implantation and TDS, there appears a peak around 1400 cm^{-1} which is attributed to mixed sp^2 and sp^3 carbon bonding as observed in amorphous SiC [30,41]. The reduction in bond connectivity by forming trigonal sp^2 carbon bonds in addition to tetrahedral sp^3 carbon is a necessary step towards amorphisation [41,42]. Annealing up to 900 °C did not recover

carbon bond disordering due to the long-range stochastic reconfiguration required to re-form a crystalline structure.

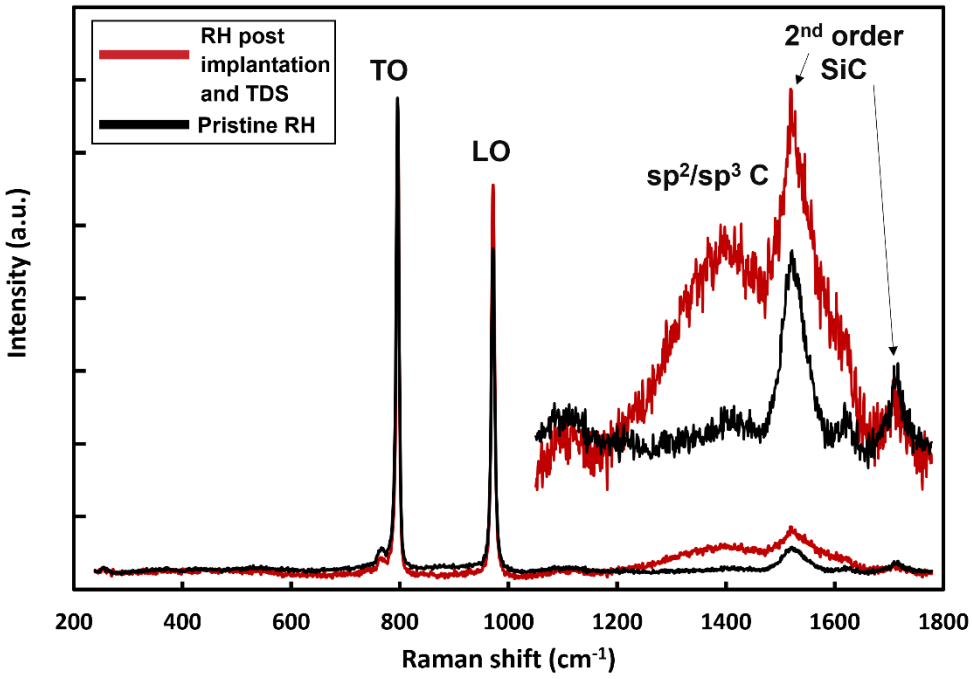

Figure 6: Raman spectra of pristine RH 3C-SiC and RH 3C-SiC following deuterium implantation and TDS. The region above 1050 cm^{-1} is shown on 7× scale. TO, LO and second order SiC peaks are labelled, along with the appearance of a peak around 1400 cm^{-1} attributed to C-C networks in amorphous SiC.

Calculations of hydrogen binding energies with vacancies

Formation energies (E_f) or solution energies (E_s) of single hydrogen atoms inserted into various defect sites were calculated, shown in Table 1. This includes substitutional sites, interstitial sites, and interstitial sites within a carbon or silicon vacancy. Hydrogen substitutions onto silicon or carbon lattice sites have very high formation energies E_f and are unfavourable to occur in combination with vacancies in a lattice. It is thermodynamically favourable to maintain the vacant site with the hydrogen atom in an interstitial position denoted by H_{TSi} for a tetrahedral silicon interstitial site, H_{TC} for a tetrahedral carbon interstitial site, and H_{ABc} for the anti-bond centre site which is the opposite vector from a Si-C tetrahedral bond direction. The $H_{TSi}V_C$ defect complex has the lowest formation energy for carbon vacancies, and the

$H_{ABc}V_{Si}$ complex is the lowest formation energy defect for silicon vacancies. The silicon vacancies have greater binding energies for hydrogen in all interstitial positions than carbon vacancies indicating that they are stronger trap sites.

Table 1: Relaxed supercell formation, binding, and solution energies of various hydrogen defect positions in SiC. Lowest formation energy defect complexes are highlighted in green.

Configuration	**E_f (eV)**	**E_b (eV)**	**E_s (eV)**
H_{Si}	8.503		
H_C	5.458		
H_{TSi}			2.805
H_{TC}			3.187
H_{BC}			2.476
H_{ABc}			2.155
$H_{TSi}V_C$	4.234	-2.912	
$H_{ABc}V_C$	4.353	-2.143	
$H_{TC}V_C$	5.261	-2.267	
$H_{ABc}V_{Si}$	6.456	-4.213	
$H_{TC}V_{Si}$	7.502	-4.198	
$H_{TSi}V_{Si}$	8.289	-3.029	

Figure 7 plots the charge density difference between a perfect crystal and two hydrogen atoms on anti-bond sites in a silicon vacancy which is surrounded by first nearest neighbour carbon atoms. This shows the localisation of electronic charge between carbon atoms and hydrogen indicating the formation of strong covalent hydrocarbon bonds. The first nearest neighbour carbon atom which is bonding to H has a distorted charge density on the opposite side, and the next nearest carbon atom's charge density is also modified by the presence of hydrogen nearby.

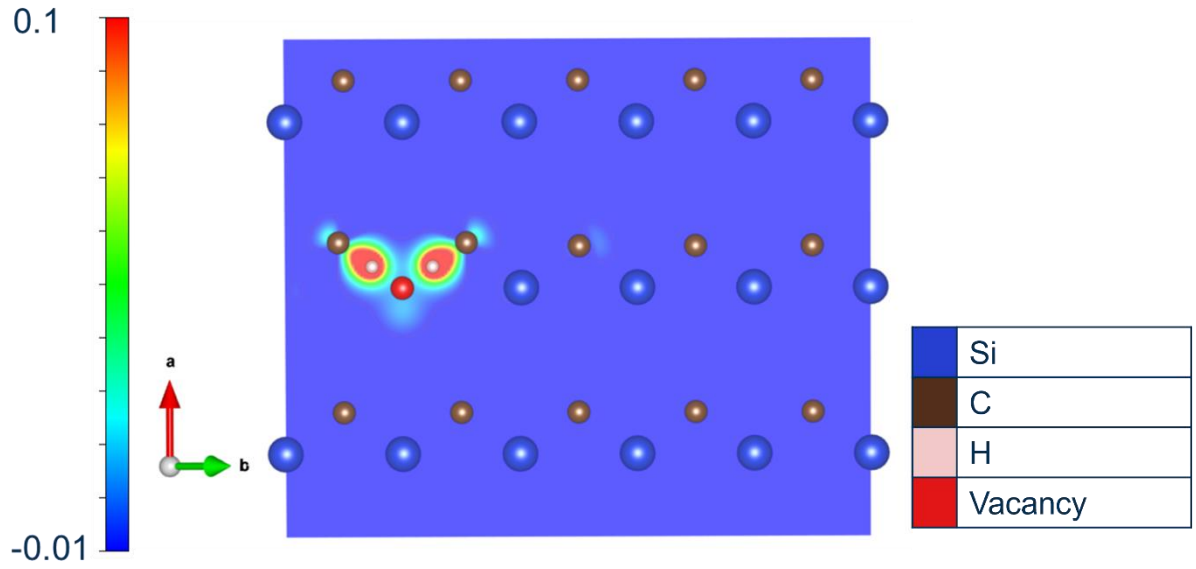

Figure 7: Plot of charge density difference relative to a perfect crystal for two hydrogen atoms in a silicon vacancy. Relative localisation of charge density is seen in the direction of carbon atoms.

Hydrogen atoms in carbon vacancies have approximately the same sequential binding energies up to 6 hydrogen atoms indicating little geometric dependency. The sequential binding energy of hydrogen atoms in a silicon vacancy remains strong for up to 4 atoms. The 5^{th} atom which is added to the silicon vacancy has an extremely small sequential binding energy, -0.142 eV. This indicates a strong 4-fold geometric dependency, potentially related to the tetrahedral C-H covalent bonding previously identified.

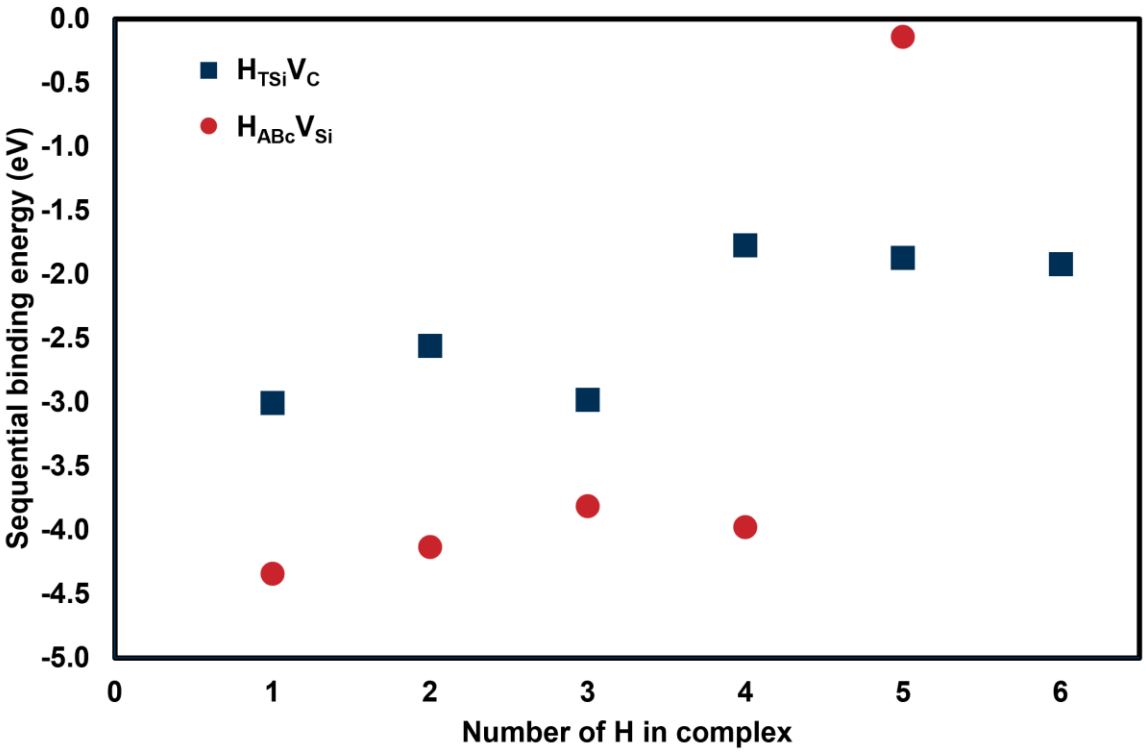

Figure 8: Sequential binding energy of multiple hydrogen atoms in carbon or silicon vacancies.

Table 2: Sequential binding energies for multiple hydrogen atoms inserted into carbon or silicon vacancies.

Number of inserted H atoms	Sequential binding energy (eV)	
	$H_{TSi}V_C$	$H_{ABc}V_{Si}$
1	-3.00	-4.34
2	-2.56	-4.13
3	-2.98	-3.81
4	-1.77	-3.98
5	-1.87	-0.14
6	-1.92	

Thermal desorption requires two steps: first de-trapping, then diffusion to a surface to be released. The lowest solution energy interstitial site for hydrogen is calculated to be the H_{ABc} position, at 2.155 eV (Table 1). The migration between H_{ABc} sites has been considered by nudged elastic band calculations. Three distinct pathways for interstitial migration have been

identified, and can be described based on Figure 9 and summarised in Table 3. Pathway 1→4 is simply switching symmetric ABc sites on the same carbon atom and has a low energy barrier. This may not necessarily be considered a migration step as the interstitial site is associated with the same atom. To be a true jump, another step is required along pathway 1→5 which is the shortest migration distance but is moving to an ABc site associated with a different carbon atom. Pathway 1→2 is a migration to another ABc site associated to a different carbon atom, but across the plane of silicon atoms and requires a longer distance displacement, but not a significantly higher energy barrier than pathway 1→5.

Table 3: Hydrogen interstitial pathways, distances, and energy barriers.

Pathway	**Distance (Å)**	**Energy barrier (eV)**
1→5	1.24	0.44
1→4	1.86	0.15
1→2	3.10	0.54

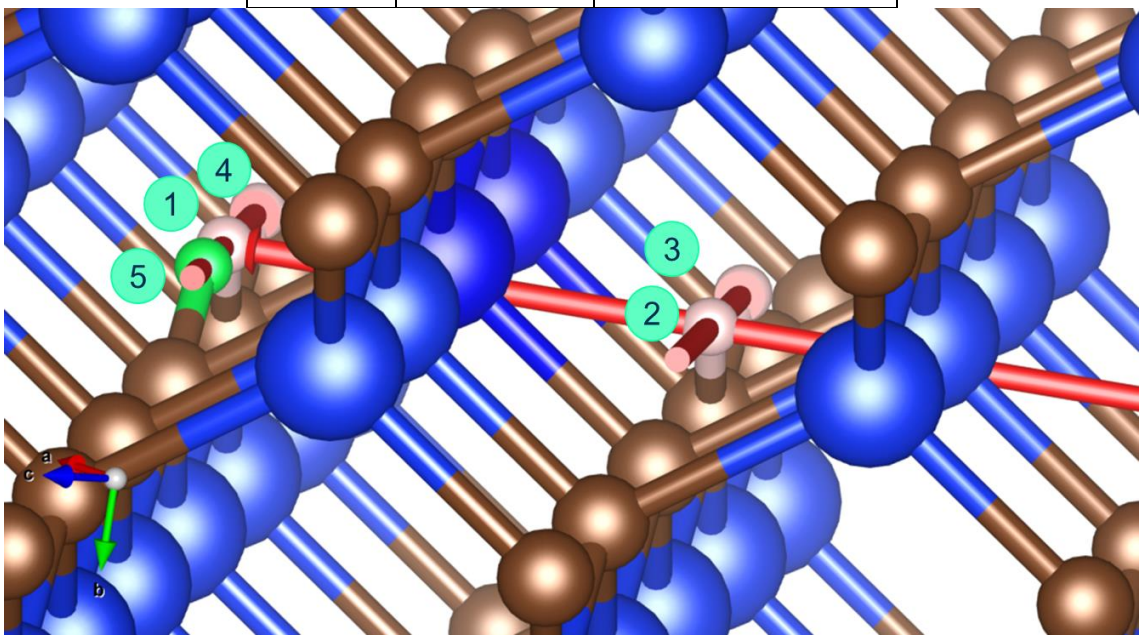

Figure 9: Hydrogen interstitial migration pathways.

Binding energies can be incorporated into an effective diffusivity (D_{eff}) using the McNabb and Foster formula (equation 5) [43,44].

$$D_{eff} = \frac{D_{perf}}{1 + (c_v) exp\left(\frac{E_b^{V-H}}{kT}\right)} \quad (5)$$

D_{perf} is the diffusivity of a perfect crystal, $D_{per} = D_0 \exp\left({}^{-E_a}/_{kT}\right)$, D_0 is the diffusion coefficient given by $D_0 = {}^{a^2 v}/_{6}$ where a is the jump length given in Table 3 for pathway 1→5 with E_a = 0.44 eV. v is a vibrational frequency based on the mass of a deuterium atom (3.32×10^{-27} kg) and the diffusion pathway energy and jump length, given by $v = \sqrt{\left({}^{2E_a}/_{ma^2}\right)}$. The vacancy concentration per atom of SiC, c_v, is estimated at 6.27×10^{-2}, for the purposes of illustration based on a defect production of ~2.7 vacancies/cm^3/neutron/cm^2 from reference [45], and the neutron fluence of the irradiated RH sample. Although c_v may be an overestimation of vacancy population as irradiations in [45] were conducted at room temperature, D_{eff} is relatively insensitive to c_v. Using calculated values, D is plotted against 1000/T in Figure 10 for a perfect 3C-SiC crystal, a polycrystal based on the diffusion equation from reference [35], and 3C-SiC containing carbon or silicon vacancies.

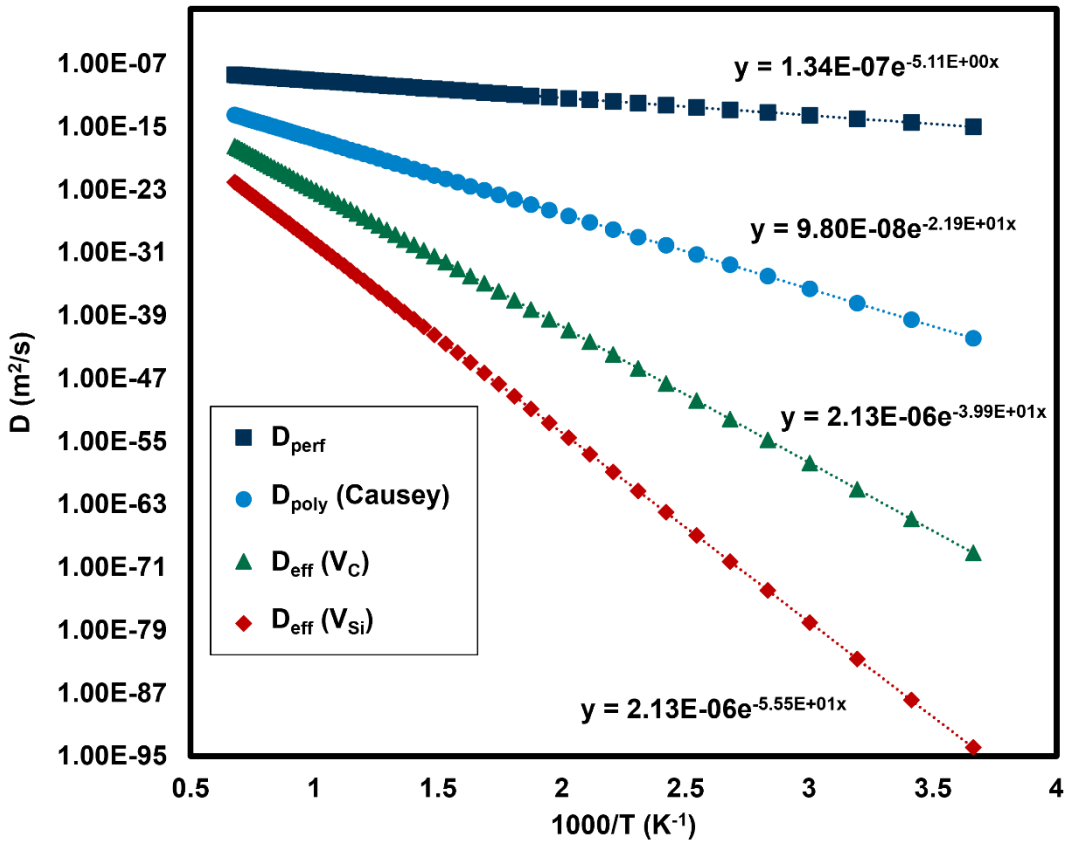

Figure 10: Calculated diffusivities for a perfect cubic crystal, a polycrystal from [35] *and 3C SiC containing carbon or silicon vacancies.*

Straight lines are fitted to the datapoints in Figure 10 to calculate effective diffusion coefficients and activation energies based on $D = D_{0,eff}\exp\left({}^{-E_{a,eff}}/_{kT}\right)$, and are given in Table 4. $D_{0,eff}$, is a function of vacancy concentration, c_v, which has been assumed as 6.27×10^{-2} in this work.

Table 4: Effective diffusion coefficients for a perfect 3C crystal, containing vacancies, and comparison to experimental polycrystal results [35].

System	$D_{0,eff}$ (m^2/s)	$E_{a,eff}$ (eV)
D_{perf}	1.34×10^{-7}	0.44
D_{eff} (vC)	2.13×10^{-6}	3.44
D_{eff} (vSi)	2.13×10^{-6}	4.78
D_{poly} [35]	9.80×10^{-8}	1.89

In summary, this set of calculations indicates very strong binding of up to 4 hydrogen atoms in a silicon vacancy, and potentially more than 6 hydrogen atoms in a carbon vacancy, but less strongly bound. Effective diffusion coefficients have been calculated for diffusion in a 3C-SiC crystal containing radiation-induced vacancies.

4. Discussion

Key results

This study has identified key differences in the retention of hydrogen isotopes in irradiated SiC, and different SiC microstructures. The neutron irradiated SiC specimen shows a single peak in deuterium release rate suggesting a specific, dominant type of trapping site, whereas unirradiated specimens of the same material have a broad temperature range of deuterium release. DFT calculations of hydrogen interaction with different vacancies shows stronger binding for hydrogen in a silicon vacancy than in a carbon vacancy, but this strong binding is limited to only 4 hydrogen atoms in the silicon vacancy, whereas carbon vacancies can accommodate at least 6 hydrogen atoms.

The microstructure of different grades of high purity 3C SiC has a measurable difference on deuterium retention; the CT specimen with high stacking fault density has lower overall deuterium retention than the RH specimen with larger grain boundary surface area. The larger high-temperature deuterium release rate from CT sample may suggest the high stacking fault density contributes relatively stronger traps for deuterium than grain boundaries. Composite specimens with open porosity have very large deuterium release rates with a broad peak potentially related to free carbon in their microstructure. The specimen where deuterium was introduced by ion implantation has a single high temperature deuterium release rate peak whereas an identical gas charged specimen has a broad deuterium release rate temperature

range beginning from lower temperatures. This suggests a modification of the specimen during ion implantation, especially when viewed in conjunction with the crystal damage observed by Raman spectroscopy. These key results will be discussed in the following sections.

Microstructural effects on hydrogen isotope trapping

The 4H SiC single crystal sample served as a reference with no grain boundaries or microstructural features allowing us to study the fundamental trapping of deuterium in SiC_4 (CSi_4) covalently bonded tetrahedral units. Although a 4H-SiC sample was used due to the difficulty of obtaining free-standing cubic single crystals, the local structure is identical to 3C-SiC (only the intermediate-range and long-range structure are slightly altered), so the retention mechanisms are likely to be similar. The single crystal has a very low retention of deuterium based on its desorption rate, suggesting that SiC either has a very low inherent trapping of deuterium, or release requires more energy than the thermal energy which was introduced in the TDS experiment here. Considering the low intrinsic deuterium retention in pristine single crystal SiC, the retention and subsequent release observed in other pristine specimens must be related to microstructural features.

The two CVD SiC specimens served as high purity monolithic specimens to investigate the effect of grain boundaries and stacking faults. The broad desorption rate peak is across the same temperature range for both samples indicating similar retention mechanisms. RH has a higher overall deuterium retention which maybe be related to the overall higher grain boundary area density than the CT sample. Grain boundaries in CVD SiC are mostly high angle boundaries which may enable faster diffusion [46]. The local chemistry of the grain boundary is likely to be important for retention of hydrogen isotopes as the binding of hydrogen to Si or C terminated surfaces of SiC wafers has different energies during hydrogenation to passivate SiC crystals [47]. Molecular dynamics simulations have shown small angle tilt boundaries are most stable with excess carbon at their core [48], and nanograins sintered in a carbon-rich

environment result in a monoplane of carbon along their boundary [49]. These effects are explained by higher interstitial mobility of carbon than of silicon or vacancies diffusion, and diffusion of carbon interstitials to grain boundaries during high temperature treatments or irradiation [48,50]. Carbon depleted grain boundaries with average 45.8at% C were observed in CVD SiC supplied by Rohm & Haas and Insaco using core loss EELS, while the carbon concentration increased following ion irradiation at 300 °C [50]. Grain boundaries are a spectrum of angles and surface terminations (whether Si or C with different energies [47]), and are likely to be sinks for impurities, which may explain the broad desorption peak. The low temperature limit of this broad peak is above the peak desorption rate temperature for purely Si-D bound deuterium, and below the peak desorption rate temperature for C-D bound deuterium. As grain boundaries are faster diffusion pathway, during the charging experiment, deuterium is likely to diffuse from the specimen surface along grain boundaries and remain in this plane. The desorption rate is highest at 700 °C for the CT sample whereas it is constant between 600 °C and 700 °C for the RH sample. This may suggest a different ratio of trap types between the CT and RH samples, potentially with a greater fraction of stronger C-D based traps in CT. The high stacking fault density of the CT sample may also contribute to strong trapping and will need further investigation of the energetics of stacking faults.

The composite sample has several orders of magnitude higher desorption rate due to the high surface area. Additionally, the composite microstructure differs from the monolithic SiC samples in having a pyrolytic carbon interface between the matrix and fibres, and the fibres which contain free carbon and impurities such as boron. CVI processing also produces a more complex matrix SiC microstructure than CVD, as the gas flow rates, temperatures, and mixtures need to be adjusted to optimise for infiltration between fibres, and deposition rate. This multi-day processing can result in different grain sizes within the specimen, along with oxidation between stages of CVI. A detailed assessment of hydrogen isotope retention in

different composite microstructures is beyond the scope of this paper. The effects of this complex microstructure are difficult to deconvolute from the single desorption rate peak maximum at 600 °C. The desorption profile from the SiC composite appears to be very similar to that from graphite reported in [19] showing the dominant effects of free carbon in the composite on deuterium retention. In a fusion reactor component, a dense layer of CVD SiC is likely to be facing the plasma or tritium breeding material so trapping by free carbon should be minimised and the results from the CVD SiC monoliths in this work are most representative.

While different microstructures of SiC and SiC composites have been studied, it is difficult to quantitatively compare our results with previous work as microstructures are not provided. While Oya and Sugiyama's work specifies cubic β-SiC, it is not clear if it is single crystal or polycrystal and what the impurities or composition might be [14,15,19,20]. Sánchez *et al.* studied reaction bonded SiC with 10% residual silicon and containing metallic impurities which create defects in both the α-SiC and silicon phases [18]. Nobuta *et al.*'s work uses a liquid phase sintered, hot pressed composite "NITE" containing alumina and yttria additives which remain as residual oxide phases in the microstructure [16,51]. It is not clear if the samples were implanted on the as-received surface or a polished surface of the composite plate. The surface preparation determines the microstructure which is exposed to the deuterium ion beam and the phases which deuterium will be implanted into. There is also no mention of trapping in residual oxide phases which tend to accumulate on grain boundaries and particularly at triple points [52]. Considering the discussion of the importance of SiC grain boundaries for retaining deuterium, the role of grain boundary phases in NITE materials will be important.

The nudged elastic band calculations show very low diffusion activation energies for hydrogen between interstitial sites, only 0.54 eV, suggesting easy diffusion of hydrogen isotopes in SiC. This is in a perfect crystal and does not include microstructural effects nor defects. This is in agreement with other literature, although negatively charged hydrogen shows

higher energy barriers [53]. Diffusion coefficients and activation energies found experimentally suggest slower diffusion, indicating microstructural effects are important at hindering the effective diffusion of hydrogen isotopes [35,54]. Strong binding energies for hydrogen to different vacancy types, in combination with low interstitial migration barriers suggests that diffusion is easy within a perfect SiC crystal, but effective diffusion can be low as hydrogen gets trapped by grain boundaries or other defects. This explains the suitability of SiC as a hydrogen permeation barrier, however may lead to strong retention of hydrogen isotopes [35,55].

Irradiation effects on hydrogen isotope trapping

The single well defined deuterium desorption rate peak at 560 °C for the neutron irradiated specimen is at lower temperature than pristine specimens, suggesting a different trapping mechanism compared to the pristine samples. As the desorption rate peak is at a lower temperature, less energy is required to detrap deuterium and diffuse it to the surface than in the pristine samples. The temperature for peak desorption rate is close to the peak desorption rate temperature for Si-D bonds proposed in the literature suggesting a change from deuterium trapping associated with carbon atoms to being associated with silicon atoms after irradiation [14,15]. The DFT calculations show smaller binding energy for hydrogen atoms to silicon atoms around a carbon vacancy than to carbon atoms around a silicon vacancy. This agrees with the experimental data where the Si-D desorption rate peak is at a lower temperature than the C-D desorption rate peaks.

The dominant point defect type for high temperature low dose irradiation is the carbon vacancy which has a high migration energy requiring annealing temperatures above ~1400 °C, whereas carbon and silicon interstitials and silicon vacancies are all mobile below 900 °C, lower than the irradiation temperature of the specimen in this work. [56,57]. The predicted preference of carbon vacancies, and the associated silicon nearest neighbours supports the

interpretation of the 560 °C desorption rate peak being associated with Si-D bonding. The absence of a high temperature desorption rate peak around 840 °C reinforces the point that silicon vacancies and their associated C-D bonding is not present in this irradiation and deuterium charging condition. There is also no broad desorption rate peak between 550 °C and 850 °C which was attributed to grain boundaries in the pristine sample. This suggests that the effective diffusivity of deuterium in SiC has been further reduced; deuterium diffuses interstitially in the grains until trapped in a carbon vacancy and before reaching a grain boundary. Alternatively, radiation damage may have modified the nature of the SiC grain boundaries as they act as defect sinks during irradiation preventing it acting as a hydrogen trap [48].

The deuterium ion implantation process could be considered as a low temperature ion irradiation experiment, causing 0.6 peak dpa of displacement damage, as shown earlier in Figure 2. Such displacement damage by deuterium implantation is not trivial in SiC, but has not been considered in previous work. The threshold amorphization dose of SiC at room temperature is below 0.5 dpa using light ions [58]. A threshold temperature depends on ion species, but is between 300-400 °C for heavy ions [59,60]. Threshold amorphization doses have been exceeded in almost all deuterium implantation experiments in the literature, however we do not know if these specimens have amorphous islands or complete amorphization. Although some researchers have conducted deuterium implantations above the threshold amorphization temperature, there is still displacement damage in their specimens which has not been characterised and may impact deuterium trapping [16–18]. Raman spectroscopy shows signs of C-C bonding even after high temperature annealing during TDS which is evidence of partial amorphisation, and significant structural damage. Below ~150 °C there is effectively no mobility for self-interstitials nor vacancies in SiC, and extended structural disordering including homonuclear C-C bonding in trigonal-tetrahedral networks may be

expected, including both sp^3 and sp^2 bonding in partially amorphized SiC. Low temperature low dose proton irradiations of SiC have been proven to create stable silicon vacancies surrounded by first nearest neighbour carbon atoms, among other defects [61,62].

The single TDS peak at ~840 °C in the Deuterium ion implanted corresponds to the C-D trapping in a carbon-rich environment proposed in [15], and no peaks corresponding to Si-D are observed. This suggests that C-D bonds are being formed during the restructuring of Si-C covalent tetrahedra into C-C homonuclear bonds in amorphous SiC, and that displacement damage is creating trapping sites during the ion implantation process which are different to those in the gas charged specimen. The desorption rate peak is quite sharp and at a higher temperature than the broad desorption rate peak in the pristine specimen. Being at a higher temperature indicates a higher binding energy for deuterium in the ion implanted specimen than in the pristine gas charged specimen, possibly related to trapping in silicon vacancies rather than at grain boundaries. Considering the low migration barrier energy for interstitial diffusion of deuterium, and the high defect density in low temperature ion implantation, implanted deuterium will be trapped to a carbon atom within a short diffusion radius and will not diffuse to a grain boundary. This mechanism explains the sharp desorption rate peak from in the deuterium ion implanted specimen. In reference [15] helium was pre-implanted to study the effects of helium in trapping sites, and displacement damage was also introduced. This helium implantation was done at room temperature where dynamic annealing is minimal and to a dose of 1×10^{18} He/cm^2 corresponding to ~40 peak dpa, almost certainly enough to (partially) amorphize the surface, or at least considerably modify the lattice with significant chemical disordering which explains the increase in their C-D signal allocated to “peak 2” for desorption from carbon-rich SiC. Amorphous SiC necessarily creates trigonal sp2 C-C bonds which may be broken up by preferential bonding with hydrogen, necessitating higher temperatures to release hydrogen. The role of helium atoms on trapping remains unclear.

Helium atoms can occupy vacancies, potentially impacting their capacity for trapping hydrogen isotopes in the subsequent deuterium implantation [63]. Further modelling work is ongoing to evaluate the interaction of helium and other transmutation produces with hydrogen and displacement defects and will experimental correlation.

The calculated binding energy of hydrogen in silicon vacancies is stronger than for hydrogen in carbon vacancies, therefore requiring more thermal energy to release. However, for more than 4 atoms in a silicon vacancy, the binding energy for subsequent hydrogen atoms is close to zero, they are effectively untrapped and will migrate to another trapping site in agreement with previous calculations by Sun *et al.* [64]. Carbon vacancies continue to trap at least 6 hydrogen atoms; Sun *et al.* calculate up to 8 atoms are stable in a carbon vacancy [64]. Considering carbon vacancies have a higher capacity for hydrogen, this may explain the sharp desorption rate peak in a narrow temperature range as hydrogen atoms are mostly bound to these traps. Silicon vacancies can only trap 4 hydrogen atoms before becoming saturated, and C-C homonuclear bonding cluster have limited C-D bonding sites, therefore at higher hydrogen concentrations as used in literature other trap types are observed including Si-D. Calculated effective diffusivities for deuterium in 3C-SiC containing vacancies are significantly lower than both the perfect crystal and polycrystal due to the strong binding of hydrogen in vacancies. This may make SiC a very good hydrogen isotope permeation barrier in an irradiation environment, however retention may be relatively large and hydrogen isotopes will remain in a grain and not necessarily diffuse to grain boundaries. The presence of other transmutation products and more complex defect structures and their influence on trapping and effective diffusion requires further investigation.

Future research opportunities

This paper has identified the importance of microstructure on deuterium trapping in SiC, and the need to further understand the retention in complex engineering composites and trapping by radiation defects produced at different temperatures. Grain boundaries are an important trap for hydrogen isotopes, and also for other radiation defects and other transmutation elements, therefore further characterisation of SiC grain boundaries should be carried out. Deuterium ion implantation has identifiably modified the structure of the material being studied, and this modification needs to be included when interpreting TDS results. Further experiments should be done to study the defects created using deuterium implantation and how these are interacting with the implanted deuterium ions as a function of dose and sample temperature. Studying neutron irradiated samples is the best for reliably understanding the damage caused to reactor components, however for deuterium retention experiments it poses challenges. Ion implantation may modify the defects in the neutron irradiated sample by creating new defects, while gas charging above the irradiation temperature will anneal radiation defects. This prevents us studying samples which have been irradiated below the deuterium gas charging temperature. During TDS radiation defects will be annealing as well as deuterium being desorbed – decoupling these effects may be challenging. However, these results will allow us to investigate stability of vacancies containing hydrogen, and potentially be more representative of a component in a fusion reactor. Neutron irradiation also produces transmutation products which will be significant in high energy fusion neutron irradiations [65,66]. Transmutation in a fission neutron spectrum is orders of magnitude lower and has not been investigated here, however future studies should look at the interaction of hydrogen isotopes with other transmutation products, including the metallic elements which can change the local charge of defects in SiC, which will impact the binding of charged forms of hydrogen [53].

5. Conclusions

A variety of SiC microstructures have been investigated for their deuterium retention properties to identify the microstructural features of most interest. Grain boundaries are the most important trapping sites in pristine polycrystalline SiC, giving a range of trapping energies and desorption temperatures. Carbon vacancies are discussed to be dominant trapping sites in high temperature neutron irradiated SiC, having a lower binding energy and thermal desorption temperature than pristine SiC. Deuterium ion implantation at room temperature could create radiation defects which include C-C homonuclear bonding structures and silicon vacancies which leads to strongly trapped deuterium as C-D bonds. DFT calculations show that hydrogen isotopes have low interstitial migration barrier energies so can diffuse easily in a perfect lattice, but vacancies are strong traps. Experimental results show that grain boundaries are also strong traps, leading to SiC being an excellent hydrogen permeation barrier, but that it could also have significant hydrogen isotope retention. Further work will be required to quantify retention in a variety of conditions and SiC microstructures, and to fundamentally understand the interaction of displacement damage and transmutation products in a fusion environment.

Acknowledgements

AJL was supported by the Royal Academy of Engineering under the Research Fellowship programme. This work was partially supported by the US Department of Energy, Office of Fusion Energy Sciences, Fusion Materials Program and Early Career Research Program under contact DE-AC05- 00OR22725 with UT-Battelle LLC. A portion of this research used resources at the HFIR, a DOE Office of Science User Facility operated by ORNL. This work has been part- funded by the EPSRC Energy Programme [grant number EP/W006839/1]. This work has been part-funded by STEP, a UKAEA programme to design and build a prototype fusion energy plant and a path to commercial fusion. DNM and IFV would like to thank

EUROfusion support for the use of high-performing computing machines: MARCONI and LEONARDO in Bologna, Italy. To obtain further information on the data and models underlying this paper please contact PublicationsManager@ukaea.uk.

References

[1] M. Lord, I. Bennett, C. Harrington, A. Cooper, D. Lee-Lane, A. Cureton, C. Olde, M. Thompson, D. Jayasundara, T. Meatyard, Fusing together an outline design for sustained fuelling and tritium self-sufficiency, Philos. Trans. R. Soc. A Math. Phys. Eng. Sci. 382 (2024). https://doi.org/10.1098/rsta.2023.0410.

[2] T. Tanabe, Tritium handling issues in fusion reactor materials, J. Nucl. Mater. 417 (2011) 545–550. https://doi.org/10.1016/j.jnucmat.2010.12.112.

[3] T. Koyanagi, Y. Katoh, T. Nozawa, L.L. Snead, S. Kondo, C.H. Henager, M. Ferraris, T. Hinoki, Q. Huang, Recent progress in the development of SiC composites for nuclear fusion applications, J. Nucl. Mater. 511 (2018) 544–555. https://doi.org/10.1016/j.jnucmat.2018.06.017.

[4] M.S. Tillack, S.A. Bringuier, I. Holmes, L. Holland, F. Santos-Novais, G.I. Maldonado, GAMBL – A dual-cooled fusion blanket using SiC-based structures, Fusion Eng. Des. 180 (2022) 113155. https://doi.org/10.1016/j.fusengdes.2022.113155.

[5] R. Pearson, C. Baus, S. Konishi, K. Mukai, A. D'Angio, S. Takeda, Overview of Kyoto Fusioneering's SCYLLA© ("Self-Cooled Yuryo Lithium-Lead Advanced") Blanket for Commercial Fusion Reactors, IEEE Trans. Plasma Sci. 50 (2022) 4406–4412. https://doi.org/10.1109/TPS.2022.3211410.

[6] G. Federici, L. Boccaccini, F. Cismondi, M. Gasparotto, Y. Poitevin, I. Ricapito, An overview of the EU breeding blanket design strategy as an integral part of the DEMO

design effort, Fusion Eng. Des. 141 (2019) 30–42. https://doi.org/10.1016/j.fusengdes.2019.01.141.

[7] S. Konishi, M. Enoeda, M. Nakamichi, T. Hoshino, A. Ying, S. Sharafat, S. Smolentsev, Functional materials for breeding blankets—status and developments, Nucl. Fusion. 57 (2017) 092014. https://doi.org/10.1088/1741-4326/aa7e4e.

[8] M. Lord, I. Bennett, C. Harrington, A. Cooper, D. Lee-Lane, A. Cureton, C. Olde, M. Thompson, D. Jayasundara, T. Meatyard, Fusing together an outline design for sustained fuelling and tritium self-sufficiency, Philos. Trans. R. Soc. A Math. Phys. Eng. Sci. 382 (2024). https://doi.org/10.1098/rsta.2023.0410.

[9] M.E. Sawan, L. Snead, S. Zinkle, Radiation damage parameters for SiC/SiC composite structure in fusion nuclear environment, Fusion Sci. Technol. 44 (2003) 150–154. https://doi.org/10.13182/FST03-A325.

[10] M.E. Sawan, Y. Katoh, L.L. Snead, Transmutation of silicon carbide in fusion nuclear environment, J. Nucl. Mater. 442 (2013) S370–S375. https://doi.org/10.1016/j.jnucmat.2012.11.018.

[11] W. Dienst, Assessment of silicon carbide as a potential wall protection material for fusion reactors, Fusion Eng. Des. 16 (1991) 311–316. https://doi.org/10.1016/0920-3796(91)90203-3.

[12] T. Abrams, S. Bringuier, D.M. Thomas, G. Sinclair, S. Gonderman, L. Holland, D.L. Rudakov, R.S. Wilcox, E.A. Unterberg, F. Scotti, Evaluation of silicon carbide as a divertor armor material in DIII-D H-mode discharges, Nucl. Fusion. 61 (2021) 66005. https://doi.org/10.1088/1741-4326/abecee.

[13] A. Widdowson, J.P. Coad, Y. Zayachuk, I. Jepu, E. Alves, N. Catarino, V. Corregidor, M. Mayer, S. Krat, J. Likonen, K. Mizohata, C. Rowley, M. Zlobinski, M. Rubel, D. Douai, K. Heinola, T. Wauters, L. Dittrich, S. Moon, P. Petersson, A. Baron-Wiechec,

L. Avotina, Evaluation of tritium retention in plasma facing components during JET tritium operations, Phys. Scr. 96 (2021). https://doi.org/10.1088/1402-4896/ac3b30.

[14] Y. Oya, Y. Hatano, M. Hara, M. Matsuyama, K. Okuno, Retention and desorption behavior of tritium in Si related ceramics, J. Nucl. Mater. 438 (2013) 22–25. https://doi.org/10.1016/j.jnucmat.2013.03.001.

[15] T. Sugiyama, Y. Morimoto, K. Iguchi, K. Okuno, M. Miyamoto, H. Iwakiri, N. Yoshida, Effects of helium irradiation on chemical behavior of energetic deuterium in SiC, J. Nucl. Mater. 307–311 (2002) 1080–1083. https://doi.org/10.1016/S0022-3115(02)01048-6.

[16] Y. Nobuta, T. Hino, Y. Yamauchi, T. Nozawa, Deuterium retention properties of SiC/SiC composites as plasma facing materials for fusion reactors after deuterium irradiation at elevated temperatures, J. Vac. Soc. Japan. 58 (2015) 173–176. https://doi.org/10.3131/jvsj2.58.173.

[17] M.T. Koller, J.W. Davis, M.E. Goodland, T. Abrams, S. Gonderman, G. Herdrich, M. Frieß, C. Zuber, Deuterium retention in silicon carbide, SiC ceramic matrix composites, and SiC coated graphite, Nucl. Mater. Energy. 20 (2019) 100704. https://doi.org/10.1016/j.nme.2019.100704.

[18] F.J. Sánchez, A. Moroño, M. Malo, E.R. Hodgson, Trapping and thermal diffusion for energetic deuterium implanted into SiC, Nucl. Mater. Energy. 9 (2016) 383–387. https://doi.org/10.1016/j.nme.2016.03.007.

[19] Y. Oya, Y. Onishi, K. Okuno, S. Tanaka, Trapping & detrapping Mech of Deuterium in SiC.pdf, 46 (2005) 552–556.

[20] Y. Oya, K. Kawaai, K. Morita, K. Iinuma, K. Okuno, S. Tanaka, Y. Makide, Retention and re-emission behavior of hydrogen isotopes in SiC, Phys. Scr. T. 103 (2002) 81–84. https://doi.org/10.1238/physica.topical.103a00081.

[21] R. Devanathan, W.. Weber, Displacement energy surface in 3C and 6H SiC, J. Nucl. Mater. 278 (2000) 258–265. https://doi.org/10.1016/S0022-3115(99)00266-4.

[22] T. Schwarz-Selinger, A critical review of experiments on deuterium retention in displacement-damaged tungsten as function of damaging dose, Mater. Res. Express. 10 (2023) 102002. https://doi.org/10.1088/2053-1591/acfdf8.

[23] J.F. Ziegler, M.D. Ziegler, J.P. Biersack, SRIM - The stopping and range of ions in matter (2010), Nucl. Instruments Methods Phys. Res. Sect. B Beam Interact. with Mater. Atoms. 268 (2010) 1818–1823. https://doi.org/10.1016/j.nimb.2010.02.091.

[24] X. Yuan, L.W. Hobbs, Modeling chemical and topological disorder in irradiation-amorphized silicon carbide, Nucl. Instruments Methods Phys. Res. Sect. B Beam Interact. with Mater. Atoms. 191 (2002) 74–82. https://doi.org/10.1016/S0168-583X(02)00516-5.

[25] L.L. Snead, S.J. Zinkle, Threshold Irradiation Dose for Amorphization of Silicon Carbide, MRS Proc. 439 (1996) 595. https://doi.org/10.1557/PROC-439-595.

[26] A. Boulle, A. Debelle, J.B. Wallace, L.B. Bayu Aji, S.O. Kucheyev, The amorphization of 3C-SiC irradiated at moderately elevated temperatures as revealed by X-ray diffraction, Acta Mater. 140 (2017) 250–257. https://doi.org/10.1016/j.actamat.2017.08.030.

[27] Y. Katoh, T. Koyanagi, J.L. McDuffee, L.L. Snead, K. Yueh, Dimensional stability and anisotropy of SiC and SiC-based composites in transition swelling regime, J. Nucl. Mater. 499 (2018) 471–479. https://doi.org/10.1016/j.jnucmat.2017.12.009.

[28] J. Li, L. Porter, S. Yip, Atomistic modeling of finite-temperature properties of crystalline β-SiC, J. Nucl. Mater. 255 (1998) 139–152. https://doi.org/10.1016/S0022-3115(98)00034-8.

[29] T. Koyanagi, Irradiation-induced chemical disordering in ceramics: The case of SiC, J.

Nucl. Mater. 565 (2022) 153766. https://doi.org/10.1016/j.jnucmat.2022.153766.

[30] N. Chaâbane, A. Debelle, G. Sattonnay, P. Trocellier, Y. Serruys, L. Thomé, Y. Zhang, W.J. Weber, C. Meis, L. Gosmain, A. Boulle, Investigation of irradiation effects induced by self-ion in 6H-SiC combining RBS/C, Raman and XRD, Nucl. Instruments Methods Phys. Res. Sect. B Beam Interact. with Mater. Atoms. 286 (2012) 108–113. https://doi.org/10.1016/j.nimb.2011.11.018.

[31] A.J. Leide, L.W. Hobbs, Z. Wang, D. Chen, L. Shao, J. Li, The role of chemical disorder and structural freedom in radiation-induced amorphization of silicon carbide deduced from electron spectroscopy and ab initio simulations, J. Nucl. Mater. 514 (2019) 299–310. https://doi.org/10.1016/j.jnucmat.2018.11.036.

[32] T. Koyanagi, J.J. Lee, J.R. Keiser, H. Gietl, Y. Katoh, Corrosion characteristics of monolithic SiC materials in beryllium-bearing molten fluoride salt, Corros. Sci. 220 (2023) 111301. https://doi.org/10.1016/j.corsci.2023.111301.

[33] A.A. Campbell, W.D. Porter, Y. Katoh, L.L. Snead, Method for analyzing passive silicon carbide thermometry with a continuous dilatometer to determine irradiation temperature, Nucl. Instruments Methods Phys. Res. Sect. B Beam Interact. with Mater. Atoms. 370 (2016) 49–58. https://doi.org/10.1016/j.nimb.2016.01.005.

[34] R.E. Stoller, M.B. Toloczko, G.S. Was, A.G. Certain, S. Dwaraknath, F.A. Garner, On the use of SRIM for computing radiation damage exposure, Nucl. Instruments Methods Phys. Res. Sect. B Beam Interact. with Mater. Atoms. 310 (2013) 75–80. https://doi.org/10.1016/j.nimb.2013.05.008.

[35] R.A. Causey, W.R. Wampler, The use of silicon carbide as a tritium permeation barrier, J. Nucl. Mater. 220–222 (1995) 823–826. https://doi.org/10.1016/0022-3115(94)00623-7.

[36] G. Kresse, J. Hafner, Ab initio molecular dynamics for liquid metals, Phys. Rev. B. 47

(1993) 558–561. https://doi.org/10.1103/PhysRevB.47.558.

[37] G. Kresse, J. Furthmüller, Efficiency of ab-initio total energy calculations for metals and semiconductors using a plane-wave basis set, Comput. Mater. Sci. 6 (1996) 15–50. https://doi.org/10.1016/0927-0256(96)00008-0.

[38] G. Kresse, J. Furthmüller, Efficient iterative schemes for ab initio total-energy calculations using a plane-wave basis set, Phys. Rev. B. 54 (1996) 11169–11186. https://doi.org/10.1103/PhysRevB.54.11169.

[39] J.P. Perdew, K. Burke, M. Ernzerhof, Generalized Gradient Approximation Made Simple, Phys. Rev. Lett. 77 (1996) 3865–3868. https://doi.org/10.1103/PhysRevLett.77.3865.

[40] P.E. Blöchl, Projector augmented-wave method, Phys. Rev. B. 50 (1994) 17953–17979. https://doi.org/10.1103/PhysRevB.50.17953.

[41] W. Bolse, Amorphization and recrystallization of covalent tetrahedral networks, Nucl. Instruments Methods Phys. Res. Sect. B Beam Interact. with Mater. Atoms. 148 (1999) 83–92. https://doi.org/10.1016/S0168-583X(98)00855-6.

[42] A.J. Leide, L.W. Hobbs, Z. Wang, D. Chen, L. Shao, J. Li, The role of chemical disorder and structural freedom in radiation-induced amorphization of silicon carbide deduced from electron spectroscopy and ab initio simulations, J. Nucl. Mater. 514 (2019) 299–310. https://doi.org/10.1016/j.jnucmat.2018.11.036.

[43] J. Sun, B.S. Li, Y.-W. You, J. Hou, Y. Xu, C.S. Liu, Q.F. Fang, Z.G. Wang, The stability of vacancy clusters and their effect on helium behaviors in 3C-SiC, J. Nucl. Mater. 503 (2018) 271–278. https://doi.org/https://doi.org/10.1016/j.jnucmat.2018.03.010.

[44] R.A. Oriani, The diffusion and trapping of hydrogen in steel, Acta Metall. 18 (1970) 147–157. https://doi.org/https://doi.org/10.1016/0001-6160(70)90078-7.

[45] V.Y. Bratus, Thermal annealing and evolution of defects in neutron-irradiated cubic SiC,

Semicond. Phys. Quantum Electron. Optoelectron. 18 (2015) 403–409. https://doi.org/10.15407/spqeo18.04.403.

[46] F. Cancino-Trejo, E. López-Honorato, R.C. Walker, R.S. Ferrer, Grain-boundary type and distribution in silicon carbide coatings and wafers, J. Nucl. Mater. 500 (2018) 176–183. https://doi.org/10.1016/j.jnucmat.2017.12.016.

[47] T. Seyller, Passivation of hexagonal SiC surfaces by hydrogen termination, J. Phys. Condens. Matter. 16 (2004) S1755–S1782. https://doi.org/10.1088/0953-8984/16/17/016.

[48] H. Jiang, X. Wang, I. Szlufarska, The Multiple Roles of Small-Angle Tilt Grain Boundaries in Annihilating Radiation Damage in SiC, Sci. Rep. 7 (2017) 42358. https://doi.org/10.1038/srep42358.

[49] S. Stelmakh, S. Gierlotka, K. Skrobas, B. Palosz, Formation of grain boundaries in nanocrystalline SiC ceramics examined by powder diffraction supported by MD simulations, J. Alloys Compd. 978 (2024) 173474. https://doi.org/10.1016/j.jallcom.2024.173474.

[50] X. Wang, H. Zhang, T. Baba, H. Jiang, C. Liu, Y. Guan, O. Elleuch, T. Kuech, D. Morgan, J.C. Idrobo, P.M. Voyles, I. Szlufarska, Radiation-induced segregation in a ceramic, Nat. Mater. 19 (2020) 992–998. https://doi.org/10.1038/s41563-020-0683-y.

[51] Y. NOBUTA, Y. YAMAUCHI, T. HINO, H.-J. CHO, H.-K. YOON, Hydrogen Retention Properties of SiC/SiC Composites as Plasma Facing Material of Fusion Reactor, J. Vac. Soc. Japan. 54 (2011) 149–151. https://doi.org/10.3131/jvsj2.54.149.

[52] K.A. Terrani, C. Ang, L.L. Snead, Y. Katoh, Irradiation stability and thermo-mechanical properties of NITE-SiC irradiated to 10 dpa, J. Nucl. Mater. 499 (2018) 242–247. https://doi.org/10.1016/j.jnucmat.2017.11.040.

[53] W. Wang, C. Li, S.L. Shang, J. Cao, Z.K. Liu, Y. Wang, C. Fang, Diffusion of hydrogen

isotopes in 3C-SiC in HTR-PM: A first-principles study, Prog. Nucl. Energy. 119 (2020) 103181. https://doi.org/10.1016/j.pnucene.2019.103181.

[54] G.A. Esteban, A. Perujo, F. Legarda, L.A. Sedano, B. Riccardi, Deuterium transport in SiCf/SiC composites, J. Nucl. Mater. 307–311 (2002) 1430–1435. https://doi.org/10.1016/S0022-3115(02)01282-5.

[55] C.H. Henager, Hydrogen permeation barrier coatings, Mater. Hydrog. Econ. (2007) 181–190. https://doi.org/10.1201/9781420006070.ch8.

[56] G. Roma, F. Bruneval, L.A. Ting, O.N. Bedoya Martínez, J.P. Crocombette, Formation and Migration Energy of Native Defects in Silicon Carbide from First Principles: An Overview, Defect Diffus. Forum. 323–325 (2012) 11–18. https://doi.org/10.4028/www.scientific.net/DDF.323-325.11.

[57] Y. Katoh, L.L. Snead, Silicon carbide and its composites for nuclear applications – Historical overview, J. Nucl. Mater. 526 (2019) 151849. https://doi.org/10.1016/j.jnucmat.2019.151849.

[58] L.L. Snead, S.J. Zinkle, Amorphization and the Effect of Implanted Ions in Sic, MRS Proc. 373 (1994) 377. https://doi.org/10.1557/PROC-373-377.

[59] X. Kerbiriou, J.M. Costantini, M. Sauzay, S. Sorieul, L. Thoṁ, J. Jagielski, J.J. Grob, Amorphization and dynamic annealing of hexagonal SiC upon heavy-ion irradiation: Effects on swelling and mechanical properties, J. Appl. Phys. 105 (2009). https://doi.org/10.1063/1.3103771.

[60] L.L. Snead, S.J. Zinkle, Threshold Irradiation Dose for Amorphization of Silicon Carbide, MRS Proc. 439 (1996) 595. https://doi.org/10.1557/PROC-439-595.

[61] A. Kawasuso, M. Yoshikawa, H. Itoh, T. Chiba, T. Higuchi, K. Betsuyaku, F. Redmann, R. Krause-Rehberg, Electron-positron momentum distributions associated with isolated silicon vacancies in 3C-SiC, Phys. Rev. B - Condens. Matter Mater. Phys. 72 (2005) 1–

6. https://doi.org/10.1103/PhysRevB.72.045204.

[62] H. Itoh, M. Yoshikawa, I. Nashiyama, S. Misawa, H. Okumura, S. Yoshida, Radiation induced defects in CVD-grown 3C-SiC, IEEE Trans. Nucl. Sci. 37 (1990) 1732–1738. https://doi.org/10.1109/23.101184.

[63] J.H. Kim, Y.D. Kwon, P. Yonathan, I. Hidayat, J.G. Lee, J.-H. Choi, S.-C. Lee, The energetics of helium and hydrogen atoms in β-SiC: an ab initio approach, J. Mater. Sci. 44 (2009) 1828–1833. https://doi.org/10.1007/s10853-008-3180-2.

[64] J. Sun, Y.W. You, J. Hou, X. Li, B.S. Li, C.S. Liu, Z.G. Wang, The effect of irradiation-induced point defects on energetics and kinetics of hydrogen in 3C-SiC in a fusion environment, Nucl. Fusion. 57 (2017). https://doi.org/10.1088/1741-4326/aa6b82.

[65] M.E. Sawan, Y. Katoh, L.L. Snead, Transmutation of silicon carbide in fusion nuclear environment, J. Nucl. Mater. 442 (2013) S370–S375. https://doi.org/10.1016/j.jnucmat.2012.11.018.

[66] M.R. Gilbert, S.L. Dudarev, D. Nguyen-Manh, S. Zheng, L.W. Packer, J.C. Sublet, Neutron-induced dpa, transmutations, gas production, and helium embrittlement of fusion materials, J. Nucl. Mater. 442 (2013) S755–S760. https://doi.org/10.1016/j.jnucmat.2013.03.085.